www.czasopisma.pan.pl PAN POLSKA AKADEMIA NAUK www.journals.pan.pl

Arch. Metall. Mater. **64** (2019), 4, 1277-1286

DOI: 10.24425/amm.2019.130091

B. DITTERT*#, M. WIESSNER**, P. ANGERER**, J.M. LACKNER***, H. LEICHTFRIED*

TAILORED Al_2O_3-Al_2TiO_5-TiO_2 COMPOSITE CERAMICS FROM DIFFERENT TITANIUM PRECURSORS

Al_2O_3-Al_2TiO_5-TiO_2 composites can be obtained by the infiltration of molecular titanium precursors into presintered α-Al_2O_3 (corundum) cylinders. Two titanium tetraalkoxides, and two dialkoxy titanium bis(acetylacetonates) serve as precursors for TiO_2 (rutile) and Al_2TiO_5 (tialite). The precursors were infiltrated as ethanolic solutions. After sintering at 1550, 1600, and 1650°C, the prepared ceramics' properties were investigated by SEM, in-situ HT-XRD, and conventional XRD. Titanium tetraisopropoxide leads to the highest content of Al_2TiO_5 in the composite. The more reactive the precursor, considering the Al_2O_3/precursor interface, the lower and more anisotropic the grain growth, the more homogeneous is the TiO_2 contribution and the higher is the content of Al_2TiO_5. Raising the sintering temperature causes an increase of the crystalline Al_2TiO_5 content as well as of the grain growth. Moreover, the reactivity of the precursor molecule influences the Ti/(Al + Ti) ratio in the obtained tialite phase.

Keywords: Composite, precursor, infiltration, alumina, tialite

1. Introduction

The properties of ceramics are strongly dependent on additives – e.g., for Al_2O_3, the addition of ZrO_2 [1], Y_2O_3-ZrO_2 [2], or TiO_2 is described [3-6]. In case of TiO_2-doping of Al_2O_3 an additional Al_2TiO_5 phase is created.

Aluminum titanate (Al_2TiO_5, tialite) is a synthetic material with a low heat conductivity [6], a low Young's modulus, a low thermal expansion coefficient and an extraordinary thermal shock resistance [7]. This combination of properties offers a wide field of applications, e.g. in metallurgy (riser pipes), in automotive engines (portliner) or for heat isolation. The mechanical properties like toughness of Al_2TiO_5 are a consequence of crack shielding of the microcrack structure. Microcracking occurs due to the anisotropic thermal expansion behavior. There is a difference between the linear, dependent on the crystallographic direction, and the averaged volumetric expansion coefficients [8]. Consequently, during cooling after sintering, microcracks occur, relaxing the formed stress peaks. In addition, doping with TiO_2 effects the properties of Al_2O_3 in different ways. Tracer diffusion experiments, carried out by Fielitz et al. [9], using ^{18}O and ^{26}Al with titanium doped α-Al_2O_3 single crystals from a Czochralski process showed that the diffusivity of Al is significantly higher in comparison to undoped Al_2O_3. The partial substitution of Al^{3+} by Ti^{4+} causes positively charged lattice defects. Consequently, Al vacancies with a high mobility occur. In case of Al_2O_3-ZrO_2 ceramics, doping with TiO_2 decreases the grade of ionicity of the Zr-O bond, and thus the diffusivity of Zr in the lattice increases. This enables the formation of liquid phases at grain boundaries, which enhance the densification behavior. A high content of TiO_2 leads to a higher content of liquid phases during the sintering process. The higher the TiO_2 content, the higher the grade of densification will be [10]. As a result, the microstructure of the obtained materials depends on the amount of titania, too. Titania promotes grain growth and, at low concentrations, the elongation of the alumina grains. The textured grains hinder grain boundary sliding and suppress superplastic deformation. However, at higher concentrations of titania, no texturing effect can be observed. Hence, grain boundary sliding, supported by the diffusion effects from the decreasing ionicity [11] due to the TiO_2 doping explained above, enables superplastic flow.

Tialite decomposes at temperatures between 900 and 1280°C [12-15] to α-Al_2O_3 and TiO_2 (rutile). Different dopants suppress the decomposition, for example MgO or mullite ($3\,Al_2O_3 \cdot 2\,SiO_2$). Corundum [16,17], however, accelerates the decomposition.

The density of the ceramics as well as the erosion resistance to molten Al can be controlled by varying the ratio of Al_2O_3 and Al_2TiO_5 [18]. Kalita and Somani [19] present Al_2O_3-Al_2TiO_5-TiO_2 composites with bioactive properties and an enhanced flexural strength.

Such composites can be obtained by the pre-synthesis and pre-calcination of powders derived from a sol-gel process from aluminum propoxide and titanium propoxide. Samples were pre-

* PROFACTOR GMBH, DEPARTMENT FUNCTIONAL SURFACES AND NANOSTRUCTURES, IM STADTGUT A2, 4407 STEYR-GLEINK, AUSTRIA
** MATERIALS CENTER LEOBEN, ROSEGGERSTRASSE 12, 8700 LEOBEN, AUSTRIA
*** JOANNEUM RESEARCH FORSCHUNGSGESELLSCHAFT MBH, INSTITUTE FOR SURFACE TECHNOLOGIES AND PHOTONICS, LEOBNER STRASSE 94, 8712 NIKLASDORF, AUSTRIA
# Corresponding author: bdittert@web.de

pared by uniaxial pressing and sintering at temperatures between 1000 and 1500°C [19, 20]. Besides self-synthesized powders, commercially available powders can be used in typical ceramic processes starting with casting, drying and sintering. Sobhani [21] started with a mixture of α-Al_2O_3 with a particle size of 700 nm, and an anatase powder of 40 nm. Ball milling followed by uniaxial pressing or wet bag isostatic pressing and sintering up to 1500°C provides the composite materials. The phase content ratios can be controlled by heating rate, soaking time and sintering temperature. Li [18] describes a comparable process.

Another method for the preparation of ceramic composites is the infiltration of precursor sols into presintered, porous ceramic bulks. The infiltration of alkoxide-derived silica and titania sols into presintered corundum [22], results in alumina-mullite-aluminum titanate composites. Corundum-mullite composites can be produced by a similiar route [23] using hydrolyzed tetraethyl orthosilicate solutions and Al_2O_3 preforms with a porosity of 65%. Al_2O_3/SiO_2 fiber composites can be obtained by the infiltration of SiO_2 sols into Al_2O_3 fiber stacks [24]. Y-doped Zirconium Toughened Alumina (ZTA) can be prepared by the infiltration of various precursor liquids of Y-Tetragonal Zirconia Polycrystal (TZP). Suspensions of nano-powders; or of nanoparticles from completely hydrolyzed propoxides of zirconium and yttrium were used as particular precursors. Partially hydrolyzed polymeric sols from propoxides of the mentioned elements were infiltrated, too [25]. Acetonic solutions of acetonates from element propoxides or pure propoxides solutions in n-propanol can be used for the infiltration. Aqueous solutions of $Zr(NO_3)_4$, and $Y(NO_3)_3$) are adequate for the infiltration of porous corundum samples. Using an aqueous nitrate solution, the infiltration step shows the highest efficiency. A presintered Al_2O_3-ZrO_2 preform is the matrix for the preparation of a Al_2O_3-ZrO_2-Al_2TiO_5 material [26] by immersion with a $TiCl_4$ solution. Stumpf et al. report about the densification of porous 3D printed cellular alumina preforms. The infiltration and coating with sols from $Al_2(OH)_5Cl$ * 2-3 H_2O lead to corundum/corundum composites [27]. Presintered 3Y-TZP specimen were used for the preparation of ZrO_2/glass composites by the infiltration of silica sols or glass slurries, respectively [28]. Al_2TiO_5 was formed in NiO/YSZ SOFC anodes by infiltration of aluminum nitrate/titanium lactate aqueous solutions, and a heat treatment at 1400°C [29]. Additionally, non-oxide ceramics like C_f/SiC-ZrC-ZrB_2 composites were produced by the infiltration of a boron containing sol into a C_f/SiC fabric followed by the infiltration of a ZrB_2 melt [30].

In this study, we use four different molecular titania precursors for the infiltration of presintered bulks made of corundum (α-Al_2O_3). Consequently, we investigated the influence on phase content and microstructure of the obtained Al_2O_3-Al_2TiO_5-TiO_2 composite ceramics. Scanning electron microscopy (SEM), and X-ray diffraction (XRD) were used for the characterization. Depending on the phase content and the microstructure, the application of the obtained materials can be the optimization of the interface to different molten metals in order to produce tailored riser pipes for metallurgy.

2. Material and Methodology

2.1. Synthesis

2.1.1. Chemicals and materials

The titanium alkoxides listed in Table 1 were purchased from ABCR (Germany), acetylacetone and ethanol were purchased from Roth/Lactan (Austria). All substances were used without further purification. Corundum hollow cylinder preforms (h = 16.9 mm, d = 13.5 mm, 3,75 g) were obtained by uniaxial pressing of commercial Al_2O_3 powder (d_{50} = 300 nm, 99,99% α-Al_2O_3) and a presinter process (850°C, 1 h). Titanium alkoxide solutions were prepared by dissolving the alkoxide in ethanol under argon atmosphere and vigorous stirring. Dialkoxytitanium bis(acetylacetonate) solutions were prepared by the addition of 2 M acetylacetone with respect to 1 mol alkoxide in ethanol similiar to the method described by Jung et al [31]. The ratio of precursor and solvent was calculated for a theoretical TiO_2 content of 10 mass% in the solution with a total weight of the whole solution of 20 g. In Table 1, the different precursors used in this work as well as the obtained sintered samples are listed.

TABLE 1

Precursors and sintering temperatures

Precursor		Ts [°C]
Titanium tetraisopropoxide	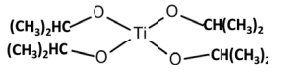	1550 1600 1650
Titanium tetra-n-butoxide	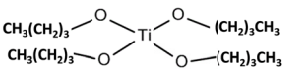	1550 1600 1650
Diisopropoxytitanium bis(acetylacetonate)	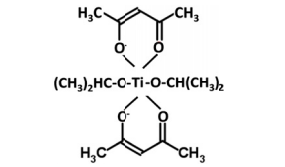	1550 1600 1650
Dibutoxytitanium bis(acetylacetonate)	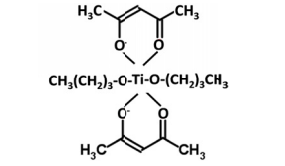	1550 1600 1650

2.1.2. Infiltration, drying and sintering

Corundum preforms were stored for 24 h in closed vessels at room temperature under air without any stirring in 20 g of the precursor solution.

After drying for 1 week in air at room temperature and a relative humidity of 30%, the cylinders were sintered in air for 2 h at 1550, 1600 and 1650°C, respectively, with a heating rate of 3°C/min.

2.2. Characterization

2.2.1. HT-XRD

The high temperature in-situ characterization experiments (HT-XRD) starting with unsintered samples were performed on a D8 Advance X-ray diffractometer (Bruker, Germany). A copper X-ray tube at 40 kV and 40 mA (Cu K_α wavelength 1.5406 Å) was used for the measurements in Bragg-Brentano beam diffraction geometry. For the detection of the diffraction intensity a 1D linear position sensitive detector (LynxEye, also by Bruker, Germany) based on the silicon strip technology was used. Each diffractogram was recorded with a step size of 0.07° in 2θ on the goniometer and 10 min total measurement time for each scan at a specific temperature (5-70° 2θ range). For the high temperature in-situ experiments, a heating rate of 1°C/s was selected. These heating experiments were performed up to a temperature of 1500°C at a heating stage HTK2000 (Paar, Austria), attached to the diffractometer. Temperature was controlled by a type S thermocouple (Pt-10% Rh / Pt) directly attached to the sample. The results were recorded both during heating and cooling phases, and a 100°C temperature increment was selected for the heating phase. All described experiments were conducted under air.

2.2.2. XRD

The conventional characterization (ex-situ) by means of the XRD method at room temperature was conducted on a D8 Discover X-ray diffractometer (Bruker, Germany) in parallel beam geometry (40 kV, 35 mA, Cu K_α radiation). This device is equipped with a Sol-X energy dispersive detector (point detector) and a polycapillary collimator. Then, the scans were performed in the range 10 to 120° 2θ with a step size of 0.03° in 2θ and a counting time of 5 s/step.

The TOPAS 5 software by Bruker AXS, Germany (1999-2014) based on the Rietveld technique [32,33] was applied for the determination of the phase content. The coherent diffracting length (which can be interpreted as a diffraction crystallite size). and the site occupancy factors of the Al and Ti atoms in the tialite phase were also investigating by using this method.

A certain part of the overall peak broadening originates from the diffractometer itself. The influence of the instrumental system on the peak broadening is determined by a calibration measurement using nearly defect free cubic lanthanum hexaboride powder [34] (NIST 660a Standard, a = 0.41569162 nm ± 0.00000097 nm). Due to the precisely known lattice parameter a of this standard, the instrumental influence on both, the peak position and the peak broadening can be determined in an accurate way. The instrumental part of the peak broadening is separated from the peak broadening resulting from the real structure by the fundamental parameter model of Cheary and Coelho [35].

The diffraction peaks are broadened by the specimen too by two types of effects concerning the real structure [36]: a) finite crystallite size and b) lattice strain (e.g. caused by dislocations). The analysis of the XRD based crystallite size (volume weighted coherent diffraction length) was conducted by the Double-Voigt-Approach as developed by Balzar [37]. This method, which is related to the older Williamson-Hall analysis uses the Scherrer equation for the size-component with the crystallite size being a refinement parameter.

Evaluation of the X-ray diffractograms by double-Voigt peak broadening model revealed that for crystalline phases the broadening due to strain effects is always small compared to broadening caused by size effects.

The area of a diffraction peak is proportional to the square of the corresponding structure factor, the phase fraction and the Lorentz-Polarisation factor (2θ – depending dwell-time and polarisation effects).

The structure factor is proportional to the average atomic form factor f as calculated in equation (1) [38]:

$$f\left(1/d\right) = occ_{\mathrm{Ti}} \cdot f_{\mathrm{Ti}}\left(1/d\right) + occ_{\mathrm{Al}} \cdot f_{\mathrm{Al}}\left(1/d\right) \tag{1}$$

d – lattice spacing parameter of the corresponding peak,
occ_{Ti} – fractional occupation of Ti,
f_{Ti} – atomic form factor of Ti,
occ_{Al} – fractional occupation of Al,
f_{Al} – atomic form factor of Al,

The atomic form factors for the Ti and Al atoms are displayed in Fig. 1 according to [38].

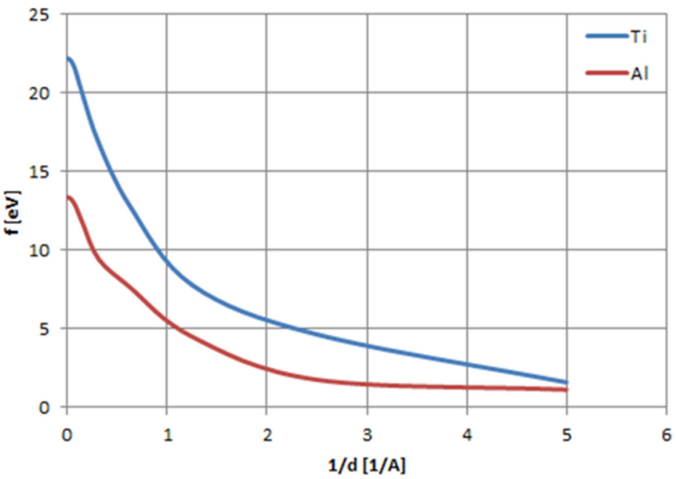

Fig. 1. Atomic form factor of Ti atoms and Al atoms as a function of the reciprocal lattice spacing

The detection limit for the Rietveld method of each phase fraction is mainly influenced by the signal-to-noise-ratio. For well crystalline phases without peak overlap [39], this limit is near 1 mass%. In the actual work this value is higher due to the lattice defects caused by the specific synthesis route of the investigated specimens. These defects induce a broader peak shape, which is correlated with a lower signal-to-noise-ratio [40] that influences the phase detection limit.

2.2.3. Backscattering scanning electron microscopy

The surface of the samples after the heating experiments was inspected to determine the grain-size by means of a scanning electron microscope (SEM) EVO MA25 (Zeiss, Germany) equipped with a lanthanum hexaboride cathode. The micrographs were recorded at a magnification of 3000x using the backscatter detector (BSD) at a voltage of 15 kV, and a working distance of 6.5 to 7.0 mm. The evaluation of these data was conducted by means of the intercept method as presented in [41].

2.2.4. Vickers indentation

The hardness of the synthetic material was tested by determination of the diagonal length of a Vickers indentation (load: 10 kgf). These measurements were conducted on a Qness Q10 A+ device (Qness, Austria). The Palmqvist fracture toughness method was performed using the related crack lengths of these indentations [42].

3. Results and discussion

3.1. Phase evolution

After sintering, dense, white, light grey or bluish cylinder samples were obtained. XRD data from Rietveld refinement show that, besides corundum, TiO_2 (rutile) as well as tialite (Al_2TiO_5) are components of the composite materials.

As presented in Fig. 2, the phase content of the obtained materials is controlled by the type of precursor and the sintering temperature. The formation of tialite according to the reaction presented in equation (2)

$$\alpha\text{-}Al_2O_3 + TiO_2\ (\text{rutile}) \rightarrow \beta\text{-}Al_2TiO_5 \qquad (2)$$

shows different grades of completion.

The infiltration of titanium tetraisopropoxide into the presintered corundum cylinders leads to a content of corundum of 76 to 78 mass% with a maximum of 78 mass% at a sintering temperature of 1600°C. Titanium tetrabutoxide causes contents of corundum of 86 to 93 mass%, with a minimum at around 86 mass% at 1600°C. When diisopropoxytitanium bis(acetylacetonate) is used as a precursor, the content of corundum was between 82 and 91 mass% with the maximum at 1600°C, and the minimum at 1650°C. The series from dibutoxytitanium bis(acetylacetonate) has corundum contents from 79 to 88 mass% showing a decreasing trend with increasing sintering temperature.

Regarding the content of rutile, the lowest content of 1 to 2 mass% occurs with using titanium tetraisopropoxide as a precursor with a decreasing trend with respect to increasing sintering temperature. Titanium tetrabutoxide leads to a rutile content of 3 to 6 mass% at 1600°C. In case of diisopropoxytitanium bis(acetylacetonate), the rutile content is between around

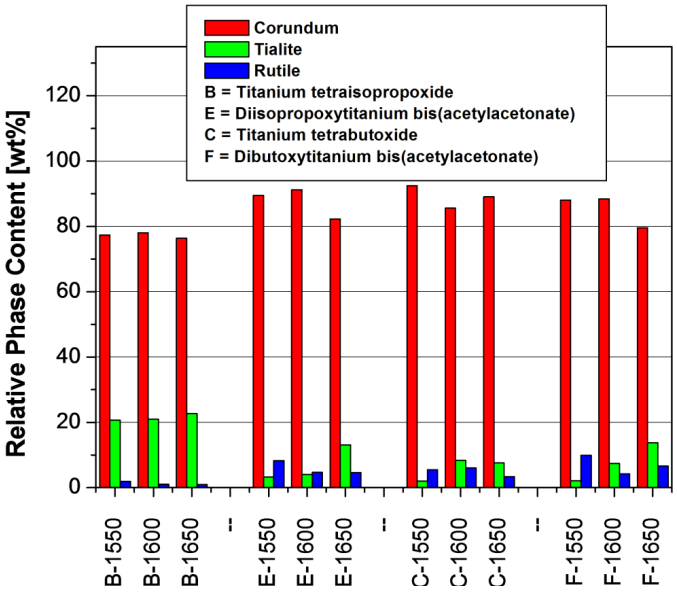

Fig. 2. Relative phase content of the obtained materials from different precursors, and sintering temperatures

4 and 5 mass% at 1650°C, and at 8 mass% at 1550°C. Using dibutoxytitanium bis(acetylacetonate), the sample contains rutile between 4 (at 1600°C) and 10 mass% at 1550°C.

Titanium tetraisopropoxide causes an extraordinary high content of tialite between 21 mass% at 1550°C, and 23 mass% at 1650°C. With titanium tetrabutoxide, tialite contents of 2 (at 1550°C) and around 8 mass% (at 1600 and 1650°C, respectively) can be obtained. Diisopropoxytitanium bis(acetylacetonate) forms materials with 3 to 13 mass% tialite with increasing sintering temperature. Titania derived from dibutoxytitanium bis(acetylacetonate) causes increasing tialite contents from 2 (1550°C) to around 14 mass% at 1650°C.

In general, the content of tialite increases with the increase of the sintering temperature in accordance with the results of Kalita and Somani [19,20]. Low [13] explained the increase of the tialite content with rising sintering temperatures by the ongoing recovery of the previously decomposed Al_2TiO_5 at temperatures above 1280°C.

Additionally, the reaction rate of equation (2) increases. The duration of the heating process time increases due to the same heating rate used for different temperatures. HT-XRD measurements of samples infiltrated with dibutoxytitanium bis(acetylacetonate) (see Fig. 3), show that there is no formation of anatase before the rutile crystallites occur from the amorphous phase. Obviously, the crystallite size of anatase was too small which comes along with massive peak broadening to be detectable by XRD. The diffraction pattern obtained at 1000°C displays clearly the occurance of the rutile phase. At 1500°C, a restructuration process correlated with the solid state reaction of rutile and corundum to tialite was observed. During the whole cooling process, a diffraction pattern of tialite can be observed. Simultaneously, the diffraction intensity of the rutile pattern is close to the detection limit of the applied HT-XRD technique.

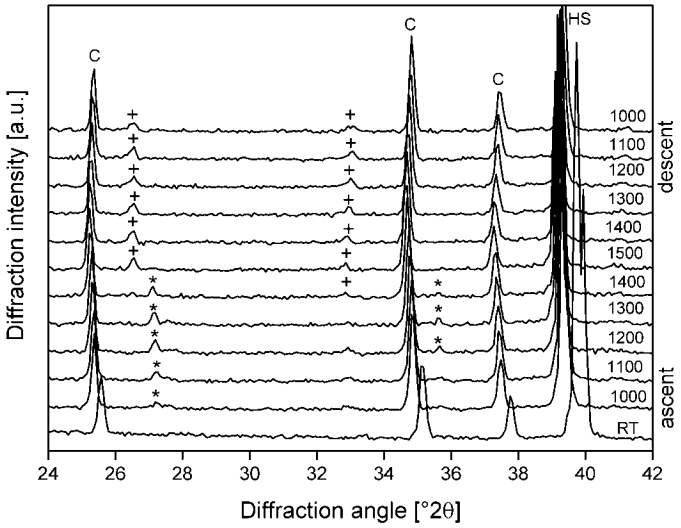

Fig. 3. Stacked plot of the diffractograms obtained during an high temperature in-situ diffraction measurement of a sample prepared with dibutoxytitanium bis(acetylacetonate). The temperature is indicated in units of °C. The symbol „C" refers to the corundum pattern, the rutile diffraction peaks are indicated by asterisks, the crosses refer to the tialite peaks, HS indicates a peak originating from the heating strip. Ascent and descent refer to the traces of the heating and the cooling phase

After the infiltration of the presintered corundum cylinders, the alkoxide precursors hydrolyze and condense due to moisture from air at the Al_2O_3 surface according to the equations (3) and (4).

$$Ti(OR)_4 + n\ H_2O \rightarrow Ti(OR)_{n-1}(OH)_n + n\ R\text{-}OH \quad (3)$$

$$2\ Ti(OR)_{n-1}(OH)_n + \rightarrow (OR)_{n-1}Ti\text{-}O\text{-}Ti(OR)_{n-1} + n\ H_2O \quad (4)$$

Besides, the alkoxide and its hydrolysis products condense to the corundum surface as described in equation (5)

$$= Al\text{-}OH + Ti(OR)_4 \rightarrow =Al\text{-}O\text{-}Ti(OR)_3 + R\text{-}OH \quad (5)$$

In all cases, an amorphous phase can be observed (see Fig. 3). The reactivity of titanium tetraisopropoxide with regard to the hydrolysis is higher than in case of the other precursors. This is a consequence of the increasing effect of sterical hindrance with the rising number of C-atoms [43] in the alkoxy group. Hence, titanium tetraisopropoxide is much more reactive [44,45], especially in presence of moisture, and hydrolyzes with a very high reaction rate that causes fast precipitation. The dialkoxytitanium bis (acetylacetonate) complex precursors are significantly less reactive due to the stronger sterical hindering effect of the acetylacetonate ligands. Additionally, the low reactivity is caused by the stability of the acetylacetonate cycle, and the delocalized p electrons. They hydrolyze very slowly and form $TiO_{0.8}(OH)_{1.6}(acac)_{0.8} \cdot 0.4H_2O$ [46] or comparable species under removal of the alkoxy groups. Besides the sterical aspect, the reactivity of titanium alkoxides and dialkoxytitanium bis (acetylacetonate) precursors is controlled by the partial charge of the Ti atom, and the ligands as well as the grade of saturation (coordination number, N). According to Blanchard [47], the ability to increase N is the most powerful factor. In Table 2, N values of the precursor molecules used in this study are presented.

TABLE 2

Coordination numbers N of the Ti atom of the different precursors

Precursor	N
Titanium tetraisopropoxide	4
Titanium tetrabutoxide	4
Diisopropoxytitanium bis(acetylacetonate)	6
Dibutoxytitanium bis(acetylacetonate)	6

Regarding all factors mentioned here, the reactivity of the different Ti compounds can be ranked as follows:

titanium tetraisopropoxide > titanium tetrabutoxide > diisopropoxytitanium bis(acetylacetonate) > dibutoxytitanium bis(acetylacetonate).

Consequently, the xerogel products formed by the reactions shown in the equations (3) to (5) have different grades of crosslinking depending on the precursor. So, the mechanism they undergo by turning to TiO_2 differs. TiO_2 from different precursors disagree with regard to the reactivity to corundum.

3.2. Microstructure

The reactivity of the precursor influences the morphology of the obtained ceramics (see Fig. 4). Backscattering scanning electron micrographs (SEM) of the cylinder surfaces of samples sintered at 1600°C, to mention two examples, disclose that the precursors have different effects on the microstructure. Titanium tetraisopropoxide forms a homogeneous structure with a low grain growth. Partially elongated corundum grains being typical for titania doped corundum according to Kebbede et al. [48] can be observed. The diffusion along grain boundaries is hindered and the growing grain is surrounded by an ultrafine matrix. Such conditions are delivered by the TiO_2 derived from titanium tetraisopropoxide. Obviously, the corundum grains are coated with the precursor during the infiltration step. The high reactivity of titanium tetraisopropoxide enables a surface reaction according to equation (5).

During the crystallization, a layer of rutile is formed around the grains, as the grey scale of the backscattering SEM indicates in Figure 4a.

In the backscattering mode of SEM, elements with higher atomic number appear brighter than elements with lower ones. In the SEM micrographs presented in this paper, titanium and aluminum are the elements of interest. The brighter the grain in the BSD SEM micrograph occurs, the more densely it is coated with titania and/or tialite. Additionally, it is smaller due to the suppressing effect of the TiO_2 layer on grain growth. The high content of tialite is a consequence of the large interface between Al_2O_3 and TiO_2. The high diffusivity of Al atoms in the presence of Ti atoms enhances the formation of tialite along the grain boundaries. The interface diffusion of Al is hindered. Thus, no significant grain growth can be observed. When titanium tetrabutoxide is used as a TiO_2 precursor, the grain growth is significantly higher than in case of titanium tetraisopropoxide.

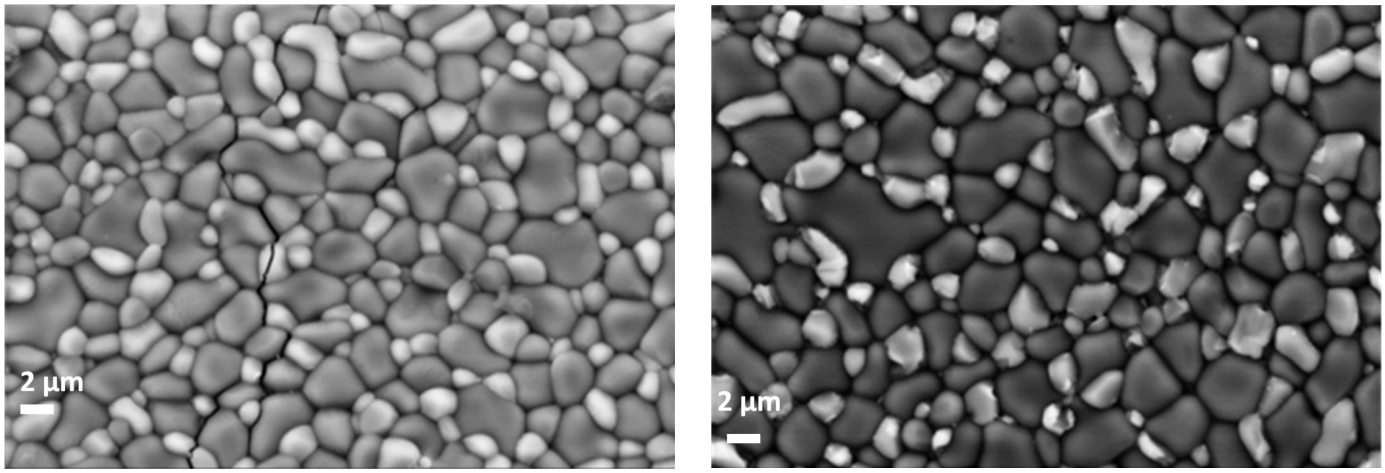

Fig. 4a. Backscattering SEM micrographs of composite materials prepared with precursors titanium tetraisopropoxide and titanium tetrabutoxide (from left to right), sintered at 1600°C

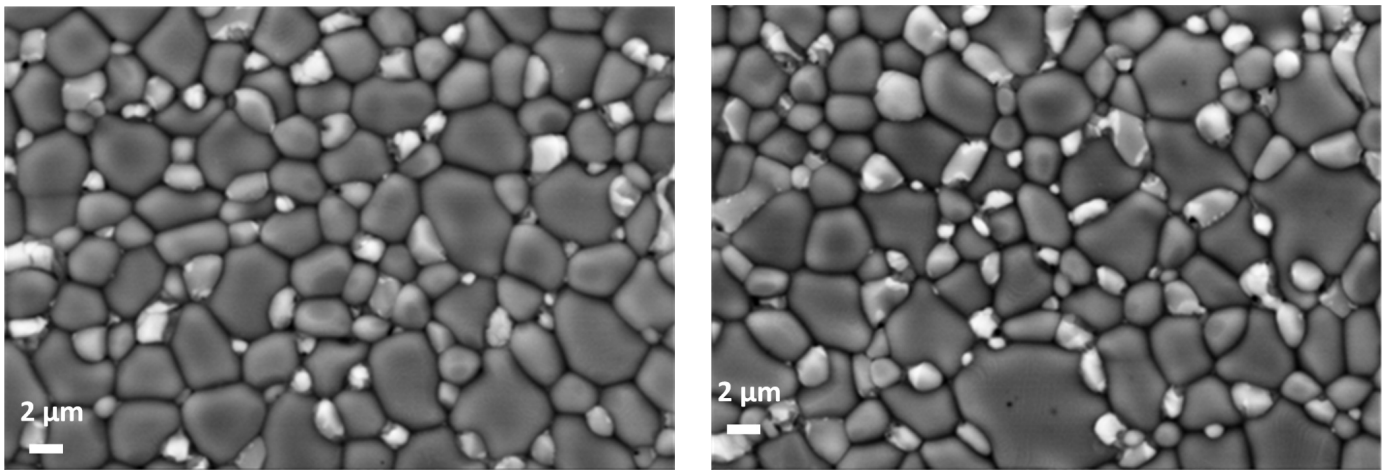

Fig. 4b. Backscattering SEM micrographs of composite materials prepared with precursors diisopropoxytitanium bis(acetylacetonate) and dibutoxytitanium bis(acetylacetonate) (from left to right), sintered at 1600°C

Furthermore, the distribution of TiO_2 in the microstructure is much less homogeneous. Corundum grains are not coated with titania, but TiO_2 is concentrated in triple points.

There is no dense layer hindering the interface diffusion causing the grain growth. Regarding the influence of the precursors diisopropoxytitanium bis(acetylacetonate) and dibutoxytitanium bis(acetylacetonate) (Fig. 4b), their hindering effect on grain growth is low, too.

Grain growth occurs unhamperedly. Grains from corundum, titania, and tialite can be observed.

The lower the reactivity of the precursor, the less homogeneous is the distribution of TiO_2 around the corundum grains. Further, the higher is the grain growth and the lower the amount of formed tialite. In Figure 5, the BSD SEM micrographs of the sample infiltrated with dibutoxytitanium bis (acetylacetonate) sintered at 1550 and 1650°C, are presented. Due to the inhomogeneous distribution of titanium in the material, no hindering effect on the grain growth can be observed. The larger grain size and the formation of tialite lead to a less homogeneous multiphasic microstructure of the material.

The mechanism of tialite formation and sintering described above is illustrated schematically in Figure 6. The distribution of TiO_2 in the presintered bodies (top row) differs. The most significant difference is, that, in case of titanium tetraisopropylate, the grains are surrounded by a layer of TiO_2. The other precursors form accumulations in the triple points of the microstructure. Consequently, the grain size of the sintered materials (bottom row) is much lower, when titanium tetraisopropoxide is used as the titanium precursor.

In Figure 7, the effect of the different titania precursors on the corundum grain size at different sintering temperatures based on the SEM data is presented. Similar to the results presented by Kalita [19] concerning Al_2O_3-Al_2TiO_5-TiO_2 composites, the mean grain size increases with a rising sintering temperature.

In comparison, the behavior of the crystallite size (coherent diffraction length) of corundum with respect to the sintering temperature and the precursor is presented in Figure 8.

In opposite to the mean grain size (see Fig. 7), for all precursors except of titanium tetraisopropoxide, the crystallite size decreases with the rising sintering temperature. According to

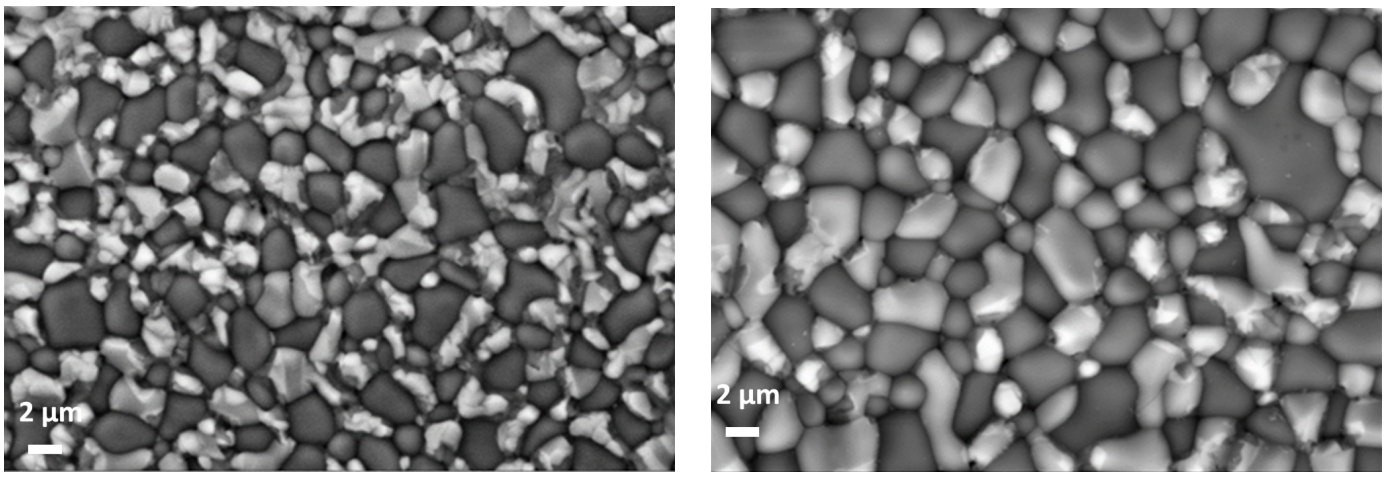

Fig. 5. Backscattering SEM micrographs of composite materials prepared with the precursors dibutoxytitanium bis(acetylacetonate) (from left to right), sintered at 1550, and 1650°C, respectively

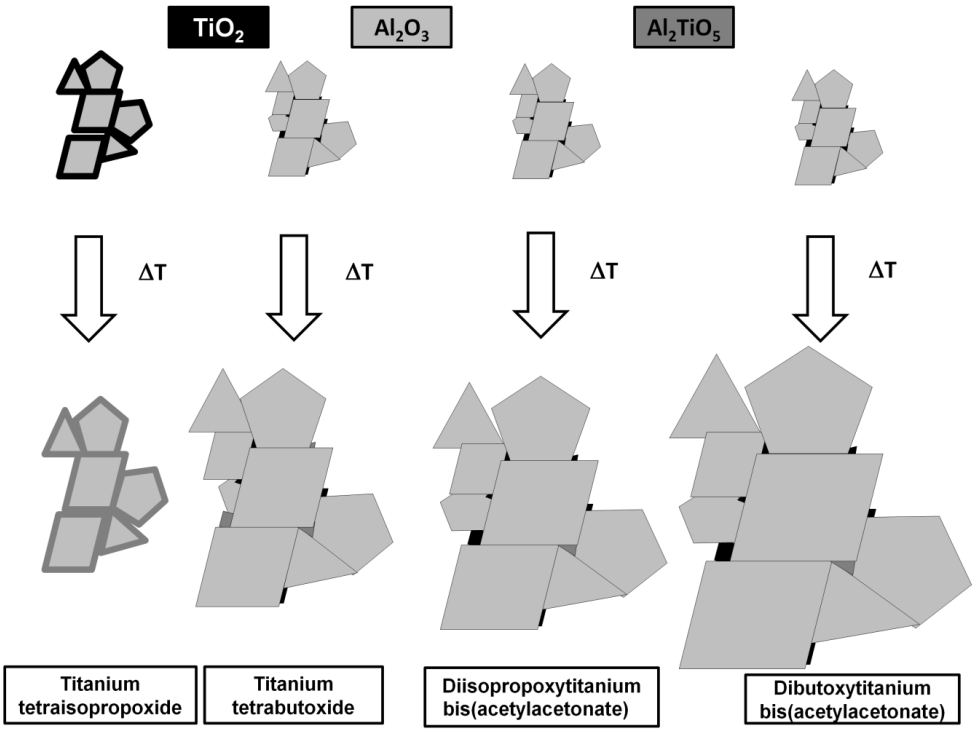

Fig. 6. Schematic presentation of the influence of the Ti precursor distribution on the microstructure evolution of the ceramics obtained by infiltration and sintering as described above. The top row shows the infiltrated and dried presintered bodies, the bottom row shows the microstructure of the ceramics with different grain sizes. The scheme shows the microstructure evolution with respect to the different precursors (columns from left to right)

equation (6), juvenile corundum crystallites are formed during the decomposition of the tialite phase. Hence, the average size of the corundum crystallites decreases.

3.3. Hardness

In case of titanium tetraisopropylate, a HV10 of 1715 can be obtained at a sintering temperature of 1550°C. At 1600°C, HV10 is 1616. With a sintering process at 1650°C, a material with a HV10 of 1679 can be obtained. Ceramic composites from titanium tetrabutylate show HV10 of 1682, 1635, and 1700 at sintering temperatures of 1550, 1600, and 1650°C, respectively. Diisopropoxytitanium (bis)acetylacetonate causes HV10 of 1666, 1684, and 1661 at 1550, 1600, and 1650°C. The use of dibutoxytitanium (bis)acetylacetonate as infiltrated precursor leads to HV10 of 1597, 1705, and 1640 at 1550, 1600, and 1650°C.

No correlation of HV10 with regard to the grain size of corundum according to the Hall-Petch relation ($H \sim \sqrt{d}$, with H = HV, d = average grain size) was observed (see Fig. 7). The Palmqvist toughness evaluation displayed also no clear correlation as well.

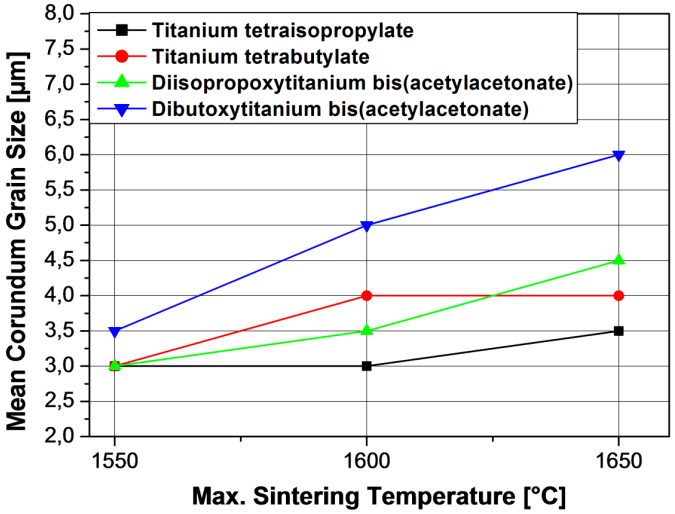

Fig. 7. Effect of the different titania precursors, and by the sintering temperature on the mean grain size of corundum as determined by SEM (intercept method)

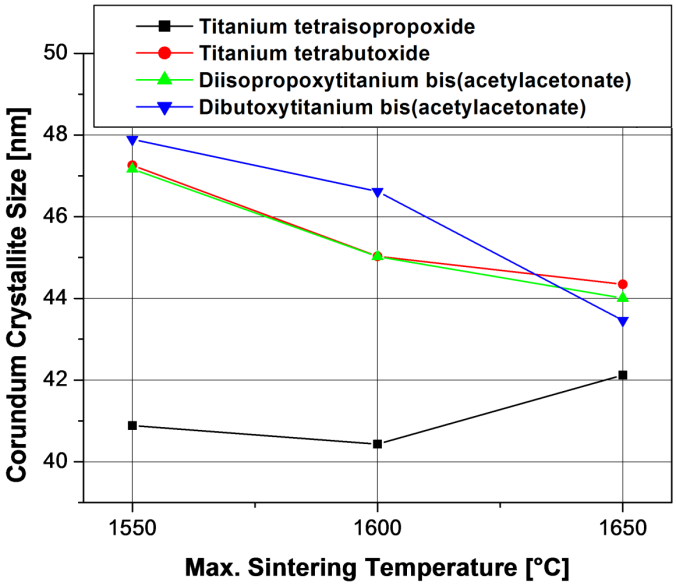

Fig. 8. Effect of the different titania precursors, and sintering temperature on the coherent diffraction length or crystallite size of corundum

3.4. Ti/(Al + Ti) ratio of the tialite phase

A deeper view shows that the Ti/(Al + Ti) ratio of the tialite phase differs with the chemistry of the precursor and sintering temperature. In Figure 9, the difference plot of a typical Rietveld refinement is displayed (Rwp = 17.7, R Bragg corundum = 7.8, R Bragg rutile = 7.0, R Bragg tialite = 8.2).

Naghizadeh et al. [49] reports about tialite-anosovite solid solutions as a product of the partial thermal decomposition of Al_2TiO_5 under the formation of juvenile Al_2O_3, and oxygen according to equation 6:

$$Al_2TiO_5 \rightarrow Al_{2(1-x)}Ti^{4+}{}_{1-(2/3)x}Ti^{3+}{}_{(2/3)x}O_{5-(10/3)x} + \\ + x\ Al_2O_3 + (x/6)\ O_2 \qquad (6)$$

In Figure 10, the increase of corundum vs. Ti/(Al + Ti) is presented. Inside the tialite phase, in case of pure Al_2TiO_5, the Ti/(Al + Ti) ratio is 0.33, in case of pure Ti_3O_5 x = 1. Even in case of the formation of corundum during the decomposition, the content of tialite is constant. Hence, the higher the titanium content of the tialite-anosovite phase, the higher is the content

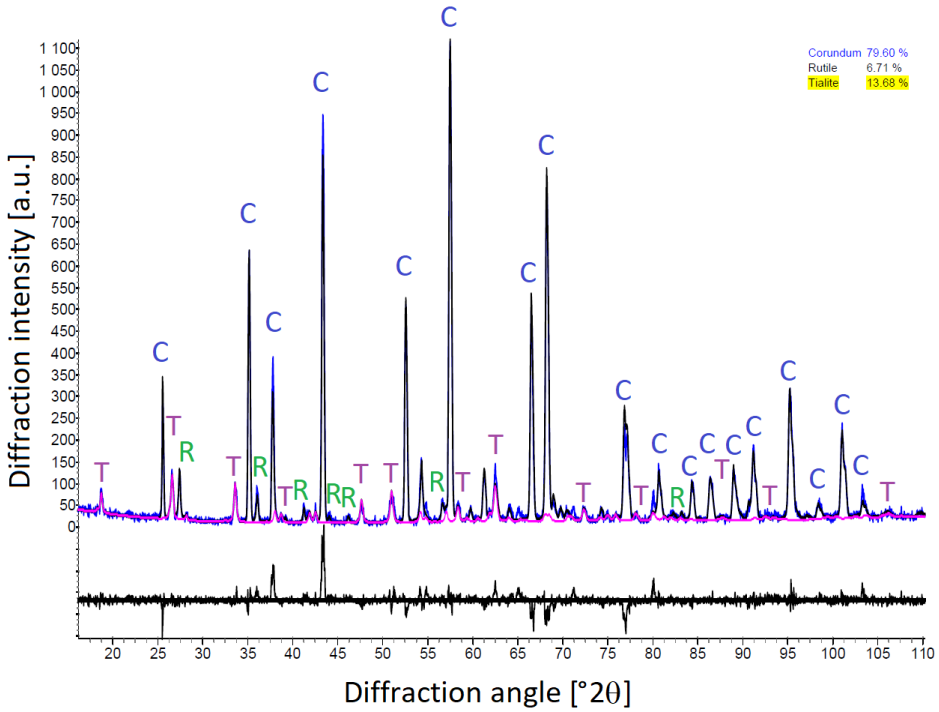

Fig. 9. Diffractogram obtained by a typical ex-situ diffraction experiment at room temperature as used for the Rietveld analysis from a sample infiltrated with dibutoxytitanium bis(acetylacetonate) and heated at 1650°C. The symbol „C“ refers to the corundum peaks, the rutile diffraction peaks are indicated by „R“, the „T“ refer to the tialite peaks. The calculated tialite pattern is highlighted

of corundum in the whole sample. The smaller crystallite size (coherent diffraction length) of the formed juvenile corundum effects the decrease shown in Figure 8. In case of titanium isopropoxide, there is a decreasing number of small corundum crystallites when the sintering temperature is raised. The crystallite growth due to the higher temperature is obviously more effective than the occurrence of juvenile corundum by the decomposition.

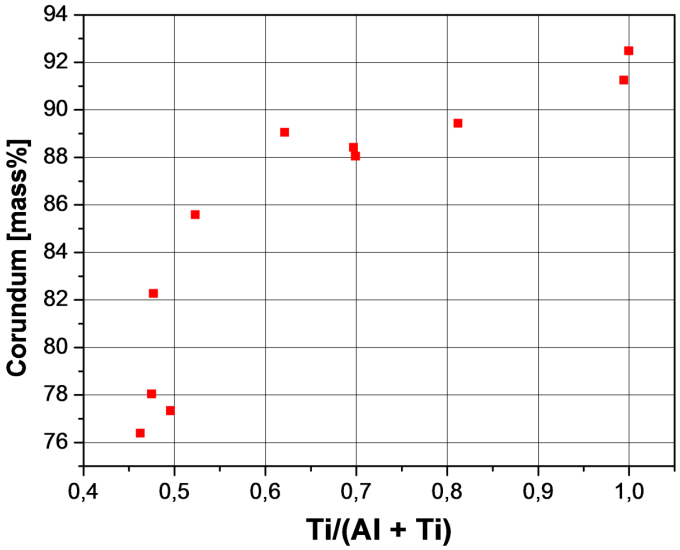

Fig. 10. Content of corundum vs. Ti/(Al + Ti)

4. Conclusion

The infiltration of different titanium alkoxide, or dialkoxytitanium bis(acetylacetonate) ethanolic solutions into porous corundum preforms leads to Al_2O_3-$Al_2Ti_2O_5$-TiO_2 composites. They differ with respect to the phase content and microstructure after sintering at 1550, 1600, and 1650°C. The content of Al_2TiO_5 is significantly higher when titanium tetraisopropoxide is used as TiO_2 precursor in comparison to other precursors. Additionally, for all precursors an increase of the Al_2TiO_5 content with the rising sintering temperature can be observed. Further, the grain growth of corundum is influenced by the titanium molecule used. Another result is that no anatase can be observed during the transformation from the precursor gel to crystalline rutile.

We show that the chemistry of the titanium precursor controls the phase content and the microstructure. In addition, the Ti/Al ratio in the tialite phase are affected by the grade of decomposition during the cooling process.

Acknowledgement

This work was supported by the Austrian Federal Government (in particular from the Bundesministerium für Verkehr, Innovation und Technologie and the Bundesministerium für Wirtschaft, Familie und Jugend, represented by Österreichische Forschungsförderungsgesellschaft mbH (FFG) within the project "SOLDOT" (grant number #834189).

REFERENCES

[1] A. Nevarez-Rascon, A. Aguilar-Elguezabal, E. Orrantia, M.H. Bocanegra-Bernal, On the wide range of mechanical properties of ZTA and ATZ based dental ceramic by varying Al_2O_3 and ZrO_2 content, Int. J. Refract. Met. H **27**, 962-970 (2009)

[2] C. Oelgardt, J. Anderson, J.G. Heinrich, G.L. Messing, Sintering, microstructure and mechanical properties of Al_2O_3-Y_2O_3-ZrO_2 (AYZ) eutectic composition ceramic microcomposites, J. Eur. Ceram. Soc. **30**, 649-656 (2010).

[3] T. Hernandez, M.C. Bautista, The role of the synthesis route to obtain densified TiO_2-doped alumina ceramics, J. Eur. Ceram. Soc. **25**, 663-672 (2005).

[4] Y. Ohya, S. Yamamoto, T. Ban, M. Tanaka, S. Kitaoka, Thermal expansion and mechanical properties of self-reinforced aluminum titanate ceramics with elongated grains, J. Eur. Ceram. Soc. **37**, 1673-1680 (2017).

[5] D. Di Marco, K. Drissi, P.M. Geffroy N. Delhote, O. Tantot, S. Verdeyme, Dielectric properties of alumina doped with TiO_2 from 13 to 73 GHz, J. Eur. Ceram. Soc. **37**, 641-646 (2017).

[6] R. Papitha, M.B. Suresh, D. Das, R. Johnson, Effect of microcracking on the thermal conductivity and thermal expansion of tialite (Al_2TiO_5) ceramics, Process Appl. Ceram. **7**, 143-146 (2013).

[7] I.J. Kim, L.J. Gauckler, Excellent thermal shock resistant materials with low thermal expansion coefficients, J. Ceram. Process Res. **9**, 240-245 (2008).

[8] Y. Ohya, Z. Nakagawa, K. Hamano, Grain-Boundary Microcracking Due to Thermal Expansion Anisotropy in Aluminum Titanate Ceramics, J. Am. Ceram. Soc. **70**, C-184-C-186 (1987).

[9] G. Fielitz, G. Borchardt, S. Ganschow, R. Bertram, A. Markwitz, ^{26}Al tracer diffusion in titanium doped single crystalline α-Al_2O_3, Solid State Ionics **179**, 373-379 (2008).

[10] Y. Zu, G. Chen,X. Fu, K. Luo, C. Wang, S. Song, W. Zhao, Effects of liquid phases on densification of TiO_2-doped Al_2O_3-ZrO_2 composite ceramics, Ceram. Int. **40**, 3989-3993 (2014)

[11] G. Chen, Y. Zu, J. Luo, X. Fu, W. Zhou, Microstructure and superplastic behavior of TiO_2-doped Al_2O_3-ZrO_2 (3Y) composite ceramics, Mater. Sci. Eng. **554**, 6-11 (2012).

[12] I.M. Low, Z. Oo, In Situ Diffraction Study of Self-Recovery in Aluminum Titanate. J. Am. Ceram. Soc. **91**, 1027-1029 (2000).

[13] I.M. Low, Z. Oo, Reformation of phase composition in decomposed aluminum titanate, Mater. Chem. Phys. **111**, 9-12 (2008).

[14] I.J. Kim, L.J. Gauckler, Formation, Decomposition and Thermal Stability of Al_2TiO_5 Ceramics, J. Ceram. Sci. Technol. **3**, 49-59 (2012).

[15] E. Kato, K. Daimon, Y. Kobayashi, Factors Affecting Decomposition Temperature of b-Al_2TiO_5. J. Ceram. Soc. Japan **86**, 626-631 (1978).

[16] V. Buscaglia, P. Nanni, Decomposition of Al_2TiO_5 and $Al_{2(1-x)}Mg_xTi_{(1+x)}O_5$ ceramics, J. Am. Ceram. Soc. **81**, 2645-2653 (1998).

[17] H.L. Lee, J.Y. Jeong, H.M. Lee, Preparation of Al_2TiO_5 from alkoxides and the effects of additives on its properties, J. Mater. Sci. **32**, 5687-5695 (1997).

[18] M. Li, F. Chen, Q. L. Shen, L. Zhang, Fabrication and thermal properties of Al_2TiO_5/Al_2O_3 composites, Mater. Sci.-Poland. **28**, 663-670 (2010).

[19] S. J. Kalita, V. Somani, Al_2TiO_5-Al_2O_3-TiO_2 nanocomposite: Structure, mechanical property and bioactivity studies, Mater. Res. Bull. **45**, 1803-1810 (2010).

[20] V. Somani, Alumina-Aluminum titanate-titania nanocomposite: Synthesis, sintering studies, assessment of bioactivity and its mechanical and electrical properties Master Thesis. Orlando, USA: University of Central Florida, 2006.

[21] M. Sobhani, T. Ebadzadeh, M.R. Rahimipour, Formation and densification behavior of reaction sintered alumina-20 wt.% aluminum titanate nano-composites, Int. J. Refract. Met. **47**, 49-53 (2014).

[22] M. Singh, I. M. Low, Depth Profiling of phase composition and preferred orientation in a graded corundum-mullite-aluminum titanate hybrid using X-ray and synchrotron radiation diffraction, Mater. Res. Bull. **37**, 1279-1291 (2002).

[23] S. Taktak, M. S. Baspinar, Wear and friction behaviour of alumina/mullite composite by sol-gel infiltration technique. Mater. Design **26**, 459-464 (2005).

[24] Z. Chengxin, C. Feng, X. Yang, P. Zhihang, Thermal shock resistance of Al_2O_3/SiO_2 composites by sol-gel, Ceramics International **45**, 11270-11274 (2019).

[25] C. Ortmann, T. Oberbach, H. Richter, P. Puhlfürß, Preparation and characterization of ZTA bioceramics with and without gradient in composition, J. Eur. Ceram. Soc. **32**, 777-785 (2012).

[26] S. Pratapa, I. M. Low, B. H. O'Connor, Infiltration-processed, functionally graded aluminium titanate/zirconia-alumina composite, J. Mater. Sci. **33**, 3037-3045 (1998).

[27] M. Stumpf, N. Travitzky, P. Greil, T. Fey, Sol-gel infiltration of complex cellular indirect 3D printed alumina, J. Eur. Ceram. Soc. **38**, 3603-3609 (2018).

[28] N.C. Ramos, M.R. Kaizer, T.M.B. Campos, J. Kim, Y. Zhang, R.M. Melo, Silica-Based Infiltrations for Enhanced Zirconia-Resin Interface Toughness, Journal of Dental Research **98**, 423-429 (2019).

[29] C. Hunt, M. Zachariasen, D. Driscoll, S. Sofie, R. Walker, Degradation rate quantification of solid oxide fuel cell performance with and without Al_2TiO_5 addition, International Journal of Hydrogen Energy **43**, 15531-15536 (2018).

[30] X. Chen, Q. Feng, H. Zhou, S. Dong, J. Wang, Y. Cao, Y. Kan, D. Ni, Ablation behavior of three-dimensional C_f/SiC-ZrC-ZrB_2 composites prepared by a joint process of sol-gel and reactive melt infiltration, Corrosion Science **134**, 49-56 (2018).

[31] M.W. Jung, H.J. Oh, J.C. Yang, Y.G. Shul, Structural Investigation of the Hydrolysis-Condensation Process of Modified Titanium Isopropoxide, Bull. Korean. Chem. Soc. **20**, 1394-1398 (1999).

[32] Bruker AXS, TOPAS V4 General profile and structure analysis software for powder diffraction data, Karlsruhe, 2005.

[33] H.M. Rietveld, A profile refinement method for nuclear and magnetic structures, J. Appl. Crystallogr. **2**, 65-71 (1969).

[34] Standard Reference Material 660a Lanthanum Hexaboride Powder Diffraction, National Institute of Standards & Technology, Gaithersburg, Maryland, (2000).

[35] R.W. Cheary, A.A. Coelho, J.P. Cline, Fundamental Parameters Line Profile Fitting in Laboratory Diffractometers, J. Res. Natl. Inst. Stand. **109**, 1-25 (2004)

[36] Diffrac plus, TOPAS/TOPAS R/TOPAS P, Version 2.1, User's Manual. Karlsruhe; 2005.

[37] D. Balzar, H. Ledbetter, Accurate modeling of size and strain broadening in the Rietveld refinement: The "double-Voigt" approach, Advances in X-Ray Analysis Plenum Press, New York, 397-404 (1995).

[38] G.K. Williamson, W.H. Hall, X-ray line broadening from filed aluminum and wolfram, Acta Metall. **1**, 22-31 (1953).

[39] International Tables for Crystallography, Volume **B**, Reciprocal Space, Edited by U. Shmueli, Second online edition, International Union of Crystallography (2010).

[40] L. Léon-Reina, M. Garcıá-Maté, G. Alvarez-Pinazo, I. Santacruz, O. Vallcorba, A.G. De la Torre, M.A.G. Aranda, Accuracy in Rietveld quantitative phase analysis: A comparative study of strictly monochromatic Mo and Cu radiations, J. Appl. Cryst. **49**, 722-735 (2016).

[41] ASTM E112-13, Standard Test Methods for Determining Average Grain Size, ASTM International, (2013).

[42] S. Palmqvist, Occurrence of crack formation during Vickers indentation as a measure of the toughness of hard materials, Archiv für das Eisenhüttenwesen **33**, 629-333 (1962).

[43] M.E. Simonsen, E.G. Søgaard, Sol-gel reactions of titanium alkoxides and water: Influence of pH and alkoxy group on cluster formation and properties of the resulting products. J. Sol-Gel Sci. Techn. **53**, 485-497 (2010).

[44] C. Sanchez, J. Livage, M. Henry, F. Babonneau, Chemical modification of alkoxide precursors, J. Non-Cryst. Solids **100**, 65-76 (1988).

[45] C. Zhou, J. Ouyang, B. Yang, Retarded hydrolysis-condensing reactivity of tetrabutyl titanate by acetylacetone and the application in dye-sensitized solar cells, Mater. Res. Bull. **48**, 4351-4356 (2013).

[46] I. Oja Acik, J. Madarász, M. Krunks, K. Tõnsuaadu, D. Janke, G. Pokol, L. Niinistö, Thermoanalytical studies of Titanium(IV) acetylacetonate xerogels with emphasis on evolved gas analysis, J. Therm. Anal. Calorim. **88**, 557-563 (2007).

[47] J. Blanchard, M. In, B. Schaudel, C. Sanchez, Hydrolysis and Condensation Reactions of Transition Metal Alkoxides: Calorimetric Study and Evaluation of the Extent of Reaction, Eur. J. Inorg. Chem. **8**, 1115-1127 (1998).

[48] A. Kebbede, G.L. Messing, A.H. Carim, Grain boundaries in titania-doped alpha-alumina with anisotropic microstructure, J. Am. Ceram. Soc. **80**, 2814-2820 (1997).

[49] R. Naghizadeh, H. R. Rezaie, F. Golestani-Fard, The influence of composition, cooling rate and atmosphere on the synthesis and thermal stability of aluminum titanate, Mater. Sci. Eng. B-Adv. **157**, 20-25 (2009).